F. Ferrari, M. Lavagna, K.C. Howell
Dynamical Model of Binary Asteroid Systems Through Patched Three-Body Problems
Celestial Mechanics and Dynamical Astronomy, Vol. 125, N. 4, 2016, p. 413-433
doi:10.1007/s10569-016-9688-x

Celestial Mechanics and Dynamical Astronomy manuscript No.
(will be inserted by the editor)

Dynamical Model of Binary Asteroid Systems Through Patched Three-Body Problems

Fabio Ferrari · Michèle Lavagna · Kathleen C. Howell

Received: date / Accepted: date

Abstract The paper presents a strategy for trajectory design in the proximity of a binary asteroid pair. A novel patched approach has been used to design trajectories in the binary system, which is modeled by means of two different three-body systems. The model introduces some degrees of freedom with respect to a classical two-body approach and it is intended to model to higher accuracy the peculiar dynamical properties of such irregular and low gravity field bodies, while keeping the advantages of having a full analytical formulation and low computational cost required. The neighborhood of the asteroid couple is split into two regions of influence where two different Three-Body Problems describe the dynamics of the spacecraft. These regions have been identified by introducing the concept of Surface Of Equivalence (SOE), a three-dimensional surface that serves as boundary between the regions of influence of each dynamical model. A case of study is presented, in terms of potential scenario that may benefit of such an approach in solving its mission analysis. Cost-effective solutions to land a vehicle on the surface of a low gravity body are selected by generating Poincaré maps on the SOE, seeking intersections between stable and unstable manifolds of the two patched three-body systems.

Keywords Binary Asteroid · Patched Three-Body Problem · Gravity Model · Surface of Equivalence · Mission Analysis · Astrodynamics

Fabio Ferrari
Department of Aerospace Science and Technology, Politecnico di Milano, Via La Masa 34, 20156 Milano, Italy
Tel.: +39 02 23998365
Fax: +39 02 23998334
E-mail: fabio1.ferrari@polimi.it

Michèle Lavagna
Department of Aerospace Science and Technology, Politecnico di Milano, Via La Masa 34, 20156 Milano, Italy
E-mail: michelle.lavagna@polimi.it

Kathleen C. Howell
School of Aeronautics and Astronautics, Purdue University, 701 W. Stadium Ave., West Lafayette, IN 47907-2045, USA
E-mail: howell@purdue.edu

1 Introduction

Since 1993, when the Galileo spacecraft flew past the asteroid Ida 243 (Belton et al 1994) and imaged its small moon Dactyl, the first natural satellite of an asteroid ever found, the interest of the scientific community on binary asteroids has grown. In the last few decades, many multiple asteroid systems have been discovered and it is currently estimated that about 16% of Near-Earth Asteroids (NEA) are binaries (Margot et al 2002; Merline et al 2002). The study of binary asteroids can be very interesting under many points of view. These kind of systems possess peculiar properties that make them good candidates for scientific and technological studies. The binary asteroid environment is the ideal place to study gravitational dynamics, to enhance the understanding of how celestial bodies in the Solar System were formed and how they evolve. In addition, it represents an ideal place for technology demonstration missions, as a test bench for In-Orbit-Demonstration (IOD) experiments. For these reasons, the study of the dynamical environment near an asteroid pair has become a relevant topic for future missions, being the focus, in particular, to the motion of a spacecraft in the neighborhood of these particular systems. One example of a mission application is the Asteroid Impact and Deflection Assessment (AIDA) mission (Cheng 2013; Cheng et al 2012), a cooperation between ESA and NASA intended to test the possibility of deflecting an asteroid on a collision path with Earth by means of a high velocity impact. AIDA mission was formed to join two different projects: the Double Asteroid Redirection Test (DART) by NASA, which will act as the kinetic impactor, and the Asteroid Impact Mission (AIM) by ESA, which will monitor the binary system before and after the impact and will operate to collect scientific data on the asteroid couple, including the deployment of a lander on the surface of the smaller asteroid. The knowledge of the dynamics driving the motion of a body in the vicinity of a binary system is then a key point for the success of the mission, to correctly operate scientific payloads and to effectively land the probe on the asteroid.

Different strategies can be adopted to model to different levels of accuracy the gravity field about asteroids (Scheeres 1994; Scheeres et al 1998; Werner and Scheeres 1997) or binary asteroid systems (Scheeres and Bellerose 2005; Gabern et al 2006; Bellerose and Scheeres 2008). Apart from the different representation of the asteroid mass distribution, all cited approaches start from the basic idea that, because of the presence of two main gravitational sources, the dynamics of a spacecraft in the proximity of a binary system can be naturally modeled with a restricted three-body problem. This consideration represents the starting point of this study as well.

The patched three-body strategy is a generalization of the classical patched conics approach (Bate et al 1971). The latter exploits a Keplerian decomposition (one attractor at the time) of the three-dimensional space, to design a trajectory in an N-body model by patching different two-body solutions. Analogously, three-body solutions can be patched together by considering two attractors at the time (Gómez et al 2004; Koon et al 2006). The transition between different gravity models is driven by the definition of regions of influence, where different models apply. To this aim, the concept of Sphere of Influence or SOI (Roy 1988), is usually adopted.

The paper proposes a novel patched approach to model the dynamics around the binary couple, using different three-body problems. The concept of SOE, in analogy with the SOI, has been developed to handle transitions between different dynamical models, with specific applications to binary asteroids. In particular, but without any loss of generality, applications related to Circular Restricted Three-Body Problem (CR3BP) are shown. The design approach and numerical methods can be easily generalized to other restricted dynamical

models (Elliptic Three-Body Problem, Full Three-Body Problem, ...), as well as to other representation of the asteroid gravity field (polyhedron, ellipsoid, ...).

The paper is organized as follows. After this introductory chapter, the main features of the CR3BP are briefly recalled in section 2. The dynamical model of the binary asteroid system is described in section 3, where the different three-body systems in use are defined and their regions of applicability are bounded according to the SOE concept, whose definition is covered in section 4. A case of study is presented in section 5 and concluding remarks are eventually reported in section 6.

2 The Circular Restricted Three-Body Problem

The main features and mathematical notation of the CR3BP, in use throughout the paper, are briefly recalled here.

The classical formulation of the Restricted Three-Body Problem considers three bodies as point masses. It studies the motion of the third body (m_3), which moves under the gravitational attraction of the other two bodies (the primaries M_1, M_2), but it does not influence their motion (restricted problem). In the Circular Restricted Three-Body Problem, the two primaries are constrained to move on circular orbits around the center of mass of the system. Since the primaries possess the same angular velocity (ω), it is useful to express the equations of motion of the third body in a reference frame that is centered in the barycenter of the two primaries and rotates together with them (Figure 1(a)). In this rotating frame, the position of the primaries is fixed and both lie on the x axis, while the system rotates with an angular velocity directed towards the positive z axis.

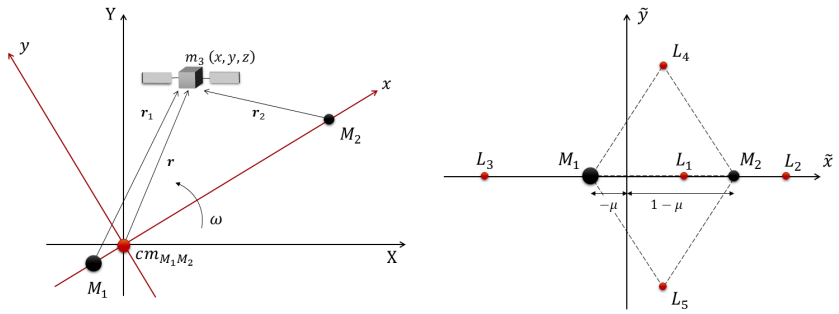

(a) (b)

Fig. 1 (a) Inertial (X,Y) and rotating (x,y) frame, (b) primaries and libration points in the rotating frame, expressed in non dimensional coordinates

As typically done, the equations of motion of the third body are written in a nondimensional form, normalized to the distance between the primaries, angular velocity and total mass of the system. In the followings, nondimensional coordinates are labeled with superscript $\tilde{}$. In a compact notation, the equations of motion read as

$$\begin{cases} \ddot{\tilde{x}} - 2\dot{\tilde{y}} = U_{\tilde{x}} \\ \ddot{\tilde{y}} + 2\dot{\tilde{x}} = U_{\tilde{y}} \\ \ddot{\tilde{z}} = U_{\tilde{z}} \end{cases} \tag{1}$$

where U is the potential function associated to the problem

$$U = \frac{1}{2}(\tilde{x}^2 + \tilde{y}^2) + \frac{1-\mu}{\tilde{r}_1} + \frac{\mu}{\tilde{r}_2} \tag{2}$$

and the notation $U_{(\cdot)}$ indicates the partial derivative of the potential function with respect to the variable $(\cdot)$. Values $\tilde{r}_1$ and $\tilde{r}_2$ represent the distances of the third body from the primaries

$$\tilde{r}_1 = \sqrt{(\tilde{x}+\mu)^2 + \tilde{y}^2 + \tilde{z}^2} \qquad \tilde{r}_2 = \sqrt{(\tilde{x}-(1-\mu))^2 + \tilde{y}^2 + \tilde{z}^2} \tag{3}$$

The parameter μ constraints the choice of the primaries. It is called mass ratio and it is defined as follows

$$\mu = \frac{M_2}{M_1 + M_2} \tag{4}$$

This problem is known to have five equilibrium points, called libration points (Figure 1(b)) and infinite periodic solutions. The interested reader can refer to Szebehely (1967); Koon et al (2006); Schaub and Junkins (2002) for full derivation of the equations of motion and further details on properties and solutions associated to the CR3BP.

3 Binary asteroid model

This section presents the assumptions made to define the dynamical model and the selection of the binary system configuration. It is known that the mass of most of known NEA binary systems is not evenly distributed among the two asteroids (Johnston 2015) being the binary couple usually made of one big asteroid (primary) and a smaller one (secondary). In this study, the big (M_1) + small (M_2) couple of asteroids (with $M_1 >> M_2$) has been chosen as reference binary system.

The dynamical model of a binary asteroid system is here built using two rotating dipoles. As mentioned in section 1, the gravity field associated to each dipole is modeled using the CR3BP formulation. The first rotating dipole is identified with the binary couple itself: the two asteroids are modeled as point masses and represent the primaries of the first three-body problem. This system will be addressed in the text as *external system*. The second rotating dipole is the result of approximating the gravity potential of the primary asteroid with the potential of two masses (two-mass concentrated model or two-mascon in the followings). These two masses are the primaries of the second three-body problem, which will be addressed as *internal system*. When considering the dynamics of the primary and secondary asteroids, this model can be seen as a simplification of the Kokoriev-Kirpichnikov problem (Gozdziewski and Maciejewski 1999), which models the planar motion of a point mass and a symmetric rigid body whose gravity field is approximated using a two-mascon model. The latest assumption makes the model appropriate to represent particular classes of bodies, such as elongated and dog-bone shaped asteroids. Recently, evidence from observations supports the idea that a large number of asteroids are made of loosely consolidated material and binaries belong to this class, as well as most of non-spherical asteroids (Richardson et al 2002). This opens to a large variety of natural bodies that are suitable to be represented with the two-mascon model. Some examples are given: 4179 Toutatis (Ostro et al 1999), 1620 Geographos (the most highly elongated body known in the solar system, Ostro et al 1995), 433 Eros (Zuber et al 2000), 951 Gaspra (Belton 1994) are examples of elongated natural bodies. Other examples can be found in asteroids 4769 Castalia (Ostro et al 1990), 2963 Bacchus (Benner et al 1999), 624 Hektor (Cruikshank et al 2000) and 216 Kleopatra (the “dogbone”

asteroid, Ostro et al 2000) that, due to their peculiar shape, are thought to be contact or close binaries and therefore their mass distribution can fit perfectly with the two-mascon model. Another example of a body whose mass distribution is likely to be modeled with the two-body mascon model is the two-lobed comet 67P/Churyumov-Gerasimenko, the target of ESA's Rosetta mission (2014). A particularly suitable candidate to be represented with the proposed patched three-body model is asteroid 243 Ida (Belton et al 1994), already identified as a good candidate for proving the dynamical properties of the Kokoriev-Kirpichnikov problem (Gozdziewski and Maciejewski 1999) with a real celestial body: asteroid 243 Ida is elongated and also, it has a small moon (Dactyl) orbiting around it.

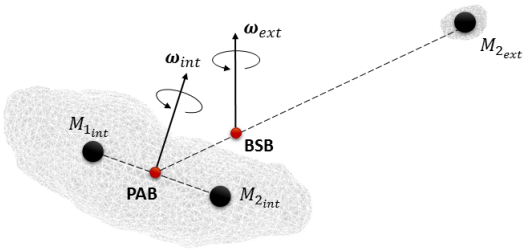

Fig. 2 Binary system in the three-dimensional space. Rotational motions around Primary Asteroid Barycenter (PAB) and Binary System Barycenter (BSB) are represented using angular velocities of the two dipoles

Figure 2 shows the orientation in the three-dimensional space of the two asteroids and the angular velocity associated to the two rotating dipoles. With reference to Figure 2, the Primary Asteroid Barycenter (PAB) and the secondary asteroid ($M_{2_{\text{ext}}}$) are the primaries of the external system (PAB is also referred as $M_{1_{\text{ext}}}$) and rotate with angular velocity $\boldsymbol{\omega}_{\text{ext}}$ around the Binary System Barycenter (BSB). On the other hand, $M_{1_{\text{int}}}$ and $M_{2_{\text{int}}}$ identify the primaries of the internal system, which rotate with angular velocity $\boldsymbol{\omega}_{\text{int}}$ about the PAB. Note that $M_{1_{\text{ext}}}$ refers to the primary asteroid, as well as the couple $M_{1_{\text{int}}}, M_{2_{\text{int}}}$ and therefore, the following relation holds

$$M_{1_{\text{ext}}} = M_{1_{\text{int}}} + M_{2_{\text{int}}} \tag{5}$$

3.1 Relative kinematics between asteroids

As shown in section 2, the nondimensional equations of motion of the third body (1), expressed in the rotating frame of a single dipole, depend only on the parameter μ. When two different rotating dipoles and their relative orientation in the 3D space are considered, other parameters must be settled to define the overall dynamical system. In particular, dimensional quantities (or common nondimensional ones) are to be considered as well as relative three-dimensional kinematics between the two systems have to be defined. The term *relative kinematics* is addressed here to indicate the relative motion between the rotation of the primary asteroid about its barycenter ($\boldsymbol{\omega}_{\text{int}}$) and the revolution of the asteroid couple (or *revolution of the secondary* in the followings) about the BSB ($\boldsymbol{\omega}_{\text{ext}}$). Reduction to special cases can be operated to the general kinematic problem. Four possible cases are identified to describe the relative kinematics between two rotating dipoles in the binary asteroid scenario.

(a) General case: the rotation of the primary is not coupled with the revolution of the secondary as the two dipoles rotate independently in the space, with $\boldsymbol{\omega}_{\text{int}}$ not aligned to $\boldsymbol{\omega}_{\text{ext}}$ and $\|\boldsymbol{\omega}_{\text{int}}\| \neq \|\boldsymbol{\omega}_{\text{ext}}\|$ (Figure 2).
(b) Planar motion: $\boldsymbol{\omega}_{\text{int}}$ is aligned to $\boldsymbol{\omega}_{\text{ext}}$, in this case the primaries of both rotating dipoles lie on the same plane. The two systems differ by a relative rotation since $\|\boldsymbol{\omega}_{\text{int}}\| \neq \|\boldsymbol{\omega}_{\text{ext}}\|$ (Figure 3).
(c) Synchronous motion: the rotation of the primary is coupled with the revolution of the secondary, but the angular velocity vectors are not aligned. The resulting patched system is periodic and the motion of the primaries is three-dimensional.
(d) Planar and synchronous motion: angular velocity vectors are equal both in magnitude and direction ($\boldsymbol{\omega}_{\text{int}} = \boldsymbol{\omega}_{\text{ext}}$). The motion of the primaries is planar and no relative rotation exists between the two rotating dipoles.

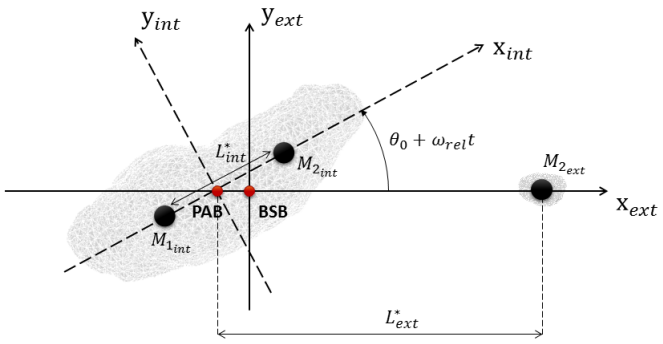

Fig. 3 Relative kinematics between internal and external dipoles (case (b), planar motion)

As previously recalled, the mass ratio μ is sufficient to retrieve the equations of motion of the CR3BP in the nondimensional rotating frame. In addition, the characteristic length L^* is required to represent the three-body system in dimensional coordinates, and the angular velocity vector is required to correctly represent the rotation of the dipole in the space. In general, when two patched CR3BP are to be considered, the full set of parameter $\{\mu, L^*, \boldsymbol{\omega}\}$ is required for each dipole, plus the information on the relative orientation of the bodies at a certain epoch (Initial Condition or IC in the followings). When special relative dynamics between the two rotating dipoles are considered (cases (b), (c) and (d)), the set of required parameters to be tuned to unequivocally define the patched CR3BP system is reduced due to constraints on the relative angular velocity. More in detail, case (b) constraints the relative orientation of the angular velocity to be null, while case (c) leaves as only degree of freedom their unitary directions ($\hat{\boldsymbol{\omega}}$). Case (d) refers to null relative angular velocity vector, both in magnitude and direction. This special case, if seen from their common rotating frame, constraints the primaries of the two dipoles to be fixed on a plane. It is a reduction of case (b), hence it can be represented with Figure 3, when the relative angular velocity $\omega_{\text{rel}} = 0$ (with $\omega_{\text{rel}} = \|\boldsymbol{\omega}_{\text{int}} - \boldsymbol{\omega}_{\text{ext}}\|$). The assumption of zero relative angular velocity between the two rotating dipoles can be done to design trajectory in the patched three-body system for slow rotating targets. In this case, the time spent on the trajectory is much less than the time the asteroid completes one rotation: hence, during the time the spacecraft flies its trajectory, the

Table 1 Set of parameters to tune the patched CR3BP system

Relative kinematics case	set of parameters		
(a) General case	$\{\mu, L^*, \boldsymbol{\omega}\}_{\text{ext}}$	$\{\mu, L^*, \boldsymbol{\omega}\}_{\text{int}}$	+IC
(b) Planar motion	$\{\mu, L^*, \|\boldsymbol{\omega}\|\}_{\text{ext}}$	$\{\mu, L^*, \|\boldsymbol{\omega}\|\}_{\text{int}}$	+IC
(c) Synchronous motion	$\{\mu, L^*, \hat{\boldsymbol{\omega}}\}_{\text{ext}}$	$\{\mu, L^*, \hat{\boldsymbol{\omega}}\}_{\text{int}}$	+IC
(d) Planar and synchronous motion	$\{\mu, L^*\}_{\text{ext}}$	$\{\mu, L^*\}_{\text{int}}$	+IC

relative position between the two asteroids in the rotating frame has not changed significantly. In the latest case, the two CR3BP are unequivocally tuned by $\{\mu_{\text{ext}}, L^*_{\text{ext}}, \mu_{\text{int}}, L^*_{\text{int}}\}$ and by selecting the IC (θ_0, with reference to Figure 3), which constraints the relative position of the four primaries. Table 1 summarize the sets of parameters to be fixed to unequivocally tune the patched CR3BP system, depending on its relative kinematics.

3.2 Dynamics of the spacecraft

The dynamical environment driving the motion of the spacecraft in the proximity of the binary system is described here. As mentioned in section 1, the classical patched conics approach considers different regions of influence, bounded by the SOI computed around a single attractor, to model the dynamics of the spacecraft. Similarly, the dynamical environment in the proximity of the binary couple is split into two regions of influence, bounded by the SOE computed around the primary asteroid. A qualitative definition of the SOE is given here. Further details on its mathematical definition and numerical computation are given in section 4.

Intuitively, it can be assumed that the dynamics of the spacecraft are dominated by the gravitational effect of the primary asteroid when it is near to it, being the effect of the smaller asteroid negligible ($M_{1_{\text{ext}}} >> M_{2_{\text{ext}}}$). This region is considered to be *internal* with respect to the SOE and the motion of the spacecraft is governed by the internal CR3BP. With reference to section 2, the equations of motion of the spacecraft are represented by system (1) and can be equivalently rewritten in vectorial form as

$$\tilde{\boldsymbol{a}}_{\text{int}} = \left\{ \begin{array}{c} 2\dot{\tilde{y}} + U_{\tilde{x}} \\ -2\dot{\tilde{x}} + U_{\tilde{y}} \\ U_{\tilde{z}} \end{array} \right\}_{\text{int}} \tag{6}$$

with notation referring to the internal nondimensional system, normalized to have unitary angular velocity (ω_{int}), total mass of the system ($M_{1_{\text{int}}} + M_{2_{\text{int}}}$) and distance between primaries.

Far from the primary asteroid, its gravity field is approximated with a simple central field, as the effects due to its non-homogeneous mass distribution are negligible. In addition, the effect of the smaller asteroid turns to be relevant as the primary field becomes weaker. This region is considered to be *external* with respect to the SOE and the dynamics of the third body is driven by the combined gravitational field of the binary couple (external CR3BP). Analogously to what done for internal system, the equations of motion of the spacecraft moving outside the SOE are represented by system (1), which in vectorial form read

$$\tilde{\boldsymbol{a}}_{\text{ext}} = \left\{ \begin{array}{c} 2\dot{\tilde{y}} + U_{\tilde{x}} \\ -2\dot{\tilde{x}} + U_{\tilde{y}} \\ U_{\tilde{z}} \end{array} \right\}_{\text{ext}} \tag{7}$$

with notation referring to the external nondimensional system, normalized to have unitary angular velocity (ω_{ext}), total mass of the system ($M_{1_{\text{ext}}} + M_{2_{\text{ext}}}$) and distance between primaries.

The schematics of the dynamical system are shown in Figure 4: the SOE represents the boundary between internal and external CR3BP.

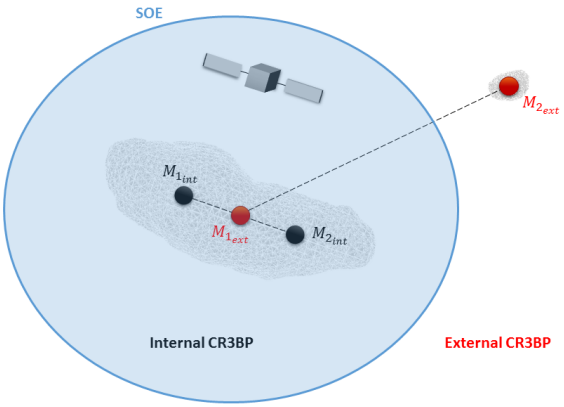

Fig. 4 Schematics of the dynamical system. SOE as boundary between regions of applicability of internal and external CR3BP

4 Surface Of Equivalence

This section discusses the mathematical definition of the SOE and its numerical computation for the case of study described in section 5. All data in use to produce results and figures presented in this paper refer to data reported in the appendix.

4.1 Definition of the SOE

The concept of Surface Of Equivalence is here developed to cover specific needs related to the study and the design of trajectories in a patched three-body model. The SOE is defined as the implicit surface

$$\mathscr{F}(\boldsymbol{G},\boldsymbol{H}) = 0 \tag{8}$$

where $\boldsymbol{G}$ and $\boldsymbol{H}$ are vector fields, as defined in section 4.2. The SOE is used to compare such vector fields and, according to the properties of the fields and by selecting the proper $\mathscr{F}(\boldsymbol{G},\boldsymbol{H})$, to establish boundaries of equivalent regions between them. The definition of the SOE here provided applies to the case of study, as shown in the followings, to compare gravity fields.

4.2 SOE to compare gravity models

A simple application of the SOE concept is shown here to compare acceleration fields associated to different gravity models. More in detail, the purpose is to identify regions in the

three-dimensional space where two different gravity models produce *equivalent* acceleration fields. It is here highlighted that *equivalent* does not mean *equal*, but it does refer to specific applications for which two acceleration fields, even if not equal, produce equivalent results according to a specified accuracy. E.g. a massive attractor can be modeled according to different mathematical models (single central field, mass distributed model, mass concentrated model, polyhedron model,...) and, depending on the specific application (e.g. distance of the spacecraft), these models can be seen as equivalent or not. It is known that the intensity of the acceleration field is inversely proportional to the square of the distance from the attractor: intuitively, different models of the same attractor can be considered equivalent far enough from the singularities of the field (gravity sources). Equivalence criteria are established through the definition of the SOE since they are directly linked with the selection of $\mathscr{F}(\boldsymbol{G},\boldsymbol{H})$.

Referring to the case of study, the SOE is here computed to confine equivalence regions between representation of primary asteroid gravity field with the single mass or with the two-mascon model. $\boldsymbol{G}$ and $\boldsymbol{H}$ represent the acceleration fields of, respectively, the two-mascon model (CR3BP, referred as $\boldsymbol{a}_{\text{int}}$, as in equation (6)) and the single mass model (Restricted Two-Body Problem, or R2BP, referred as $\boldsymbol{a}_{2B}$). It is convenient to evaluate both acceleration fields in the rotating frame associated to the two-mascon model (referred as internal system in section 3), such that the asteroid remains fixed in the space. In this particular reference frame, vector fields are time-invariant and their functional expression read as

$$\boldsymbol{G} = \boldsymbol{G}(x,y,z) \qquad \boldsymbol{H} = \boldsymbol{H}(x,y,z)$$

To facilitate the comparison between acceleration fields, dimensional units are used. More in detail, the dimensional form of equation (6) can be written as

$$\boldsymbol{a}_{\text{int}} = \left\{ \begin{array}{c} \omega_{\text{int}}^2 x + 2\omega_{\text{int}}\dot{y} - G\left(\frac{M_{1_{\text{int}}}}{r_1^3}(x+x_1) + \frac{M_{2_{\text{int}}}}{r_2^3}(x-x_2)\right) \\ \omega_{\text{int}}^2 y - 2\omega_{\text{int}}\dot{x} - Gy\left(\frac{M_{1_{\text{int}}}}{r_1^3} + \frac{M_{2_{\text{int}}}}{r_2^3}\right) \\ -Gz\left(\frac{M_{1_{\text{int}}}}{r_1^3} + \frac{M_{2_{\text{int}}}}{r_2^3}\right) \end{array} \right\}_{\text{int}} \tag{9}$$

where x,y,z refer to the dimensional coordinates in the internal CR3BP, x_1, x_2 represent the position of the two primaries on the x axis, r_1, r_2 the distance of the third body from the primaries and G is the universal gravitational constant.

The contribution due to the single mass representation of the primary, in the rotating frame reads as

$$\boldsymbol{a}_{2\text{B}} = \left\{ \begin{array}{c} \omega_{\text{int}}^2 x + 2\omega_{\text{int}}\dot{y} - G\frac{M_{1_{\text{int}}}+M_{2_{\text{int}}}}{r^3}x \\ \omega_{\text{int}}^2 y - 2\omega_{\text{int}}\dot{x} - G\frac{M_{1_{\text{int}}}+M_{2_{\text{int}}}}{r^3}y \\ -G\frac{M_{1_{\text{int}}}+M_{2_{\text{int}}}}{r^3}z \end{array} \right\}_{\text{int}} \tag{10}$$

with r representing the distance of the spacecraft from the barycenter of the system.

Since the vector field is being evaluated with spacecraft at rest ($\dot{x} = \dot{y} = \dot{z} = 0$), Coriolis terms in equations (9) and (10) result to be zero and then equations can be simplified into the form in use to define the SOE:

$$\boldsymbol{a}_{\text{int}} = \left\{ \begin{array}{c} \omega_{\text{int}}^2 x - G\left(\frac{M_{1_{\text{int}}}}{r_1^3}(x+x_1) + \frac{M_{2_{\text{int}}}}{r_2^3}(x-x_2)\right) \\ \omega_{\text{int}}^2 y - Gy\left(\frac{M_{1_{\text{int}}}}{r_1^3} + \frac{M_{2_{\text{int}}}}{r_2^3}\right) \\ -Gz\left(\frac{M_{1_{\text{int}}}}{r_1^3} + \frac{M_{2_{\text{int}}}}{r_2^3}\right) \end{array} \right\}_{\text{int}} = \boldsymbol{G}(x,y,z) \tag{11}$$

and

$$\boldsymbol{a}_{2\mathrm{B}} = \left\{ \begin{array}{c} \omega_{\mathrm{int}}^2 x - G\frac{M_{1_{\mathrm{int}}}+M_{2_{\mathrm{int}}}}{r^3}x \\ \omega_{\mathrm{int}}^2 y - G\frac{M_{1_{\mathrm{int}}}+M_{2_{\mathrm{int}}}}{r^3}y \\ -G\frac{M_{1_{\mathrm{int}}}+M_{2_{\mathrm{int}}}}{r^3}z \end{array} \right\}_{\mathrm{int}} = \boldsymbol{H}(x,y,z) \tag{12}$$

4.3 SOE example: relative difference in magnitude

In this paragraph, the SOE is computed by comparing the magnitude of different acceleration fields. Figure 5(a) shows contour lines of the function $f(x,y,z)$, which represents the relative difference in magnitude between fields

$$f(x,y,z) = \frac{\|\boldsymbol{a}_{\mathrm{int}} - \boldsymbol{a}_{2B}\|}{\|\boldsymbol{a}_{\mathrm{int}}\|} \tag{13}$$

The value of f in each point (x,y,z) of the domain corresponds to the difference in magnitude between central field and two-mascon model as percentage of the latter. As expected, the difference between the fields is maximum near the asteroid and decreases monotonically moving away from it.

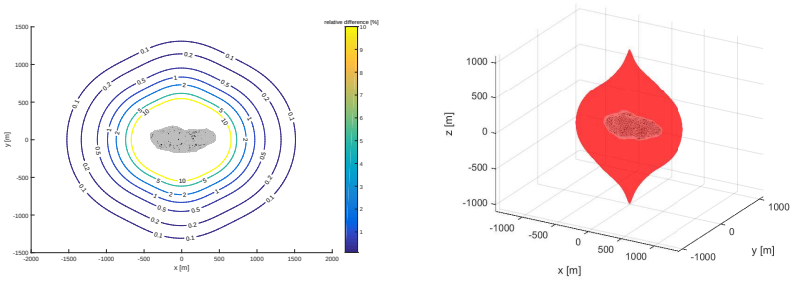

(a) (b)

Fig. 5 (a) Contour lines of function $f(x,y,z)$ (eq. (13)): projection on x,y plane. Relative difference in magnitude expressed as percentage of $\|\boldsymbol{a}_{\mathrm{int}}\|$. (b) Three-dimensional view of the SOE (with $\kappa = 5\%$). Magnitude of acceleration fields is compared

Equation (13) is included in the definition of the SOE (8), which is expressed as the implicit surface

$$\mathscr{F}(\boldsymbol{G},\boldsymbol{H}) = \frac{\|\boldsymbol{G}-\boldsymbol{H}\|}{\|\boldsymbol{G}\|} - \kappa = 0 \tag{14}$$

or equivalently

$$\frac{\|\boldsymbol{a}_{\mathrm{int}} - \boldsymbol{a}_{2B}\|}{\|\boldsymbol{a}_{\mathrm{int}}\|} = \kappa \tag{15}$$

being κ a scalar value representing the norm of the vectorial difference between the fields normalized to $\|\boldsymbol{a}_{\mathrm{int}}\|$ or, in other words, the percentage of difference between the models. The analytical expression of the SOE can be written in the dimensional rotating frame by substituting equations (11) and (12) into equation (15): it results into a nonlinear scalar equation to be solved for the value κ. Figure 5(b) shows the three-dimensional SOE computed

for $\kappa = 5\%$. As mentioned, the SOE bounds regions of equivalence of different models, according to a specific accuracy. In this case, as it appears clear from Figure 5(a), the SOE divides the domain into two regions: the internal region (where $f > 5\%$) and the external region (where $f < 5\%$). A region of *equivalence* between the two models, within the accuracy of 5%, is then identified outside the SOE.

4.4 SOE example: relative difference in direction

Other SOEs can be computed according to different equivalence criteria. The equivalence of two acceleration fields can be assessed in terms of vector orientation (other than vector magnitude). In analogy to what done for the case of magnitude comparison, the relative difference in direction between fields is defined as $g(x,y,z)$

$$g(x,y,z) = \arccos\left(\frac{\boldsymbol{a}_{\text{int}} \cdot \boldsymbol{a}_{2B}}{\|\boldsymbol{a}_{\text{int}}\|\|\boldsymbol{a}_{2B}\|}\right) \tag{16}$$

Figure 6(a) shows contour lines of the function $g(x,y,z)$ being the relative difference in directions, expressed in degrees, between the vector fields under study. Again, the difference between the fields is maximum near the asteroid and decreases away from it.

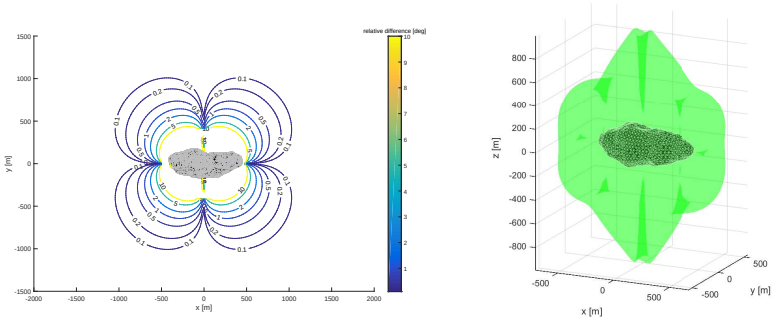

(a) (b)

Fig. 6 (a) Contour lines of function $g(x,y,z)$ (eq. (16)): projection on x,y plane. Relative difference in direction expressed in degrees. (b) Three-dimensional view of the SOE (with $\gamma = 2^\circ$). Direction of acceleration fields is compared

In this case, the SOE is defined as

$$\arccos\left(\frac{\boldsymbol{a}_{\text{int}} \cdot \boldsymbol{a}_{2B}}{\|\boldsymbol{a}_{\text{int}}\|\|\boldsymbol{a}_{2B}\|}\right) = \gamma \tag{17}$$

being γ the angle between vectors of the different fields. Figure 6(b) shows the three-dimensional SOE computed when $\gamma = 2^\circ$. In analogy to the magnitude comparison case, the region of *equivalence* between the two models, within the accuracy of 2°, is identified outside the SOE.

5 Case of Study

The following section presents a study case of a landing scenario for an exploration mission to a NEA binary system. The patched three-body strategy described in this paper is here adopted to design the landing trajectory of a space probe. The relative kinematics of the target binary system is firstly described, with reference to section 3.1. The dynamical environment is modeled according to assumptions made in section 3.2, using the SOE concept defined in section 4. The case of study refer to data reported in the appendix.

5.1 Relative kinematics of the binary system

The study case presented here refer to the simplest case in terms of relative kinematics between asteroids among those presented in section 3.1: it is assumed that planar and synchronous motion applies for the binary system under study (case (d)). This assumption simplifies the computations but it does not affect the validity and meaningfulness of the design process. The relative kinematics of the binary systems do not affect the motion of the two rotating dipoles and therefore the applicability of the CR3BP in their domain of interest: relative kinematics between asteroids are important only at the SOE, where the transition between internal and external CR3BP occurs instantaneously. In this respect, case (d) is equivalent to the general non-synchronous and three-dimensional motion (case (a)), with the two rotating dipoles aligned only during transition at the SOE. Moreover, a simpler study case fits better than a more complex case with the needs of showing and explaining a novel design approach, which is the ultimate goal of the paper. The patched approach shown here can be easily applied to any general, more complex study case.

As shown in Table 1, when case (d) applies, the patched three-body system is tuned by fixing the following set $\boldsymbol{P}$ of parameters (with reference to Figure 3)

$$\boldsymbol{P} = \{\mu_{\text{ext}}, L^*_{\text{ext}}, \mu_{\text{int}}, L^*_{\text{int}}, \theta_0\} \tag{18}$$

The set $\boldsymbol{P}$ is selected according to the target binary system and refer to characteristics of both binary couple and primary asteroid. Parameters related to the external system μ_{ext} and L^*_{ext} refer to the asteroid couple since they represent the mass ratio between the two asteroids and relative distance between them. Parameters of the internal system μ_{int} and L^*_{int} are the degrees of freedom to model the gravity field of the primary asteroid: the mass ratio and distance of the two masses is used to approximate the mass distribution of the natural body. Last, θ_0 fixes the relative position of the four primaries $\{M_{1_{\text{ext}}}, M_{2_{\text{ext}}}, M_{1_{\text{int}}}, M_{2_{\text{int}}}\}$ in their common rotating frame. Values of $\boldsymbol{P}$ refer to Table 4 in the appendix. The target binary configuration is shown in Figure 7: all primaries are collinear and lie on the x axis of the common rotating frame. According to Scheeres (2004), if two asteroids are modeled as ellipsoids, the smaller asteroid being aligned with the minimum inertia axis of the primary represents an equilibrium configuration, which can be of stable equilibrium depending on the values of angular momentum, mass ratio and inertia properties of the asteroid couple. The design case under study is however found to stay in the region of instability, due to the chosen mass ratio between the asteroids. Nevertheless, the choice of the configuration is justified by the fact that the two dipoles interacts dynamically only during transition at SOE: from the particle dynamics point of view, this patched model can be representative of the case in which the primaries move with a general non-synchronous, three-dimensional motion (case (a)), with instantaneous transition at SOE during alignment of the dipoles. The relative kinematics do

not affect the dynamics of internal and external CR3BP in their domain and, since the transition at the SOE between patched three-body problems is instantaneous, the rotating dipoles need to be aligned only when the spacecraft is at the SOE.

Two ellipsoids are used to approximate the surface of the asteroids to design the landing trajectory and for visualization.

5.2 Dynamical environment

The spacecraft moves in the proximity of the asteroid couple following the dynamics described in section 3.2. The computation of the SOE to confine internal and external system is here presented for the study case.

Section 4 presents the mathematical definition of the SOE and shows some examples of its computation around the primary asteroid. The magnitude of vectors between two different acceleration fields are compared and serve to define condition (8) to compute the SOE. The results shown in section 4 are applied to the binary system case and used to compute the SOE for the case of study presented here: inside the SOE the dynamics are driven by the internal CR3BP (being the smaller asteroid negligible), outside the SOE the dynamics are driven by the external CR3BP, being the primary modeled as single mass.

The case of study considers the magnitude SOE (Figure 5(b)) computed in section 4. The surface is defined as

$$\frac{\|\boldsymbol{a}_{\text{int}} - \boldsymbol{a}_{2B}\|}{\|\boldsymbol{a}_{\text{int}}\|} = \kappa \tag{19}$$

with the threshold value κ in use in section 4:

$$\kappa = 5\% \tag{20}$$

This value has been selected with the goal of satisfying constraints on the geometry of the problem (SOE not smaller than primary asteroid and not bigger than the binary system) while keeping a satisfactory representation of the dynamics: the internal three-body system is considered as the real world model to represent the primary asteroid and the SOE represents a boundary after which the gravity contribution of the primary is modeled to a lower accuracy (if SOE is too small the accuracy of the model of the primary is too low, if the SOE is too big the effect of the secondary inside it is too high to be discarded). Since the differences in magnitude decreases by moving away from the primary asteroid (Figure 5(a)), outside the SOE the acceleration fields satisfy condition

$$\frac{\|\boldsymbol{a}_{\text{int}} - \boldsymbol{a}_{2B}\|}{\|\boldsymbol{a}_{\text{int}}\|} < \kappa \tag{21}$$

meaning that, outside the SOE, the acceleration fields are *equivalent*, within the accuracy specified in (20).

Figure 7 shows the dynamical environment in use to support trajectory design in the case of study. It is here shown the x,y projection of the SOE, splitting the neighborhood of the binary couple into two regions where internal and external CR3BP apply. Libration points of both internal and external systems are shown.

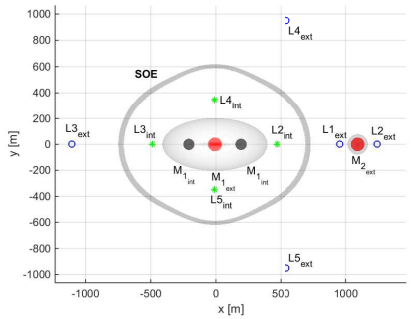

Fig. 7 Dynamical system, with two CR3BP and their libration points in the rotating frame: green stars indicate libration point of the internal system, blue circles indicate libration points of the external system

5.3 Mission analysis with patched three-body approach

An example of how the patched three-body system can be employed to support the mission analysis design of a potential mission scenario is presented. Cost-effective solutions to land a vehicle on the surface of the primary asteroid are selected by exploiting manifold dynamics of the two three-body systems whose interaction has been resolved by means of Poincaré maps analysis on the SOE.

The mission scenario considers a spacecraft initially following a periodic orbit about the L1 point of the external CR3BP. During the landing phase, the spacecraft follows the dynamics of the external system to reach the SOE and then, after transition to internal CR3BP, it reaches the surface of the primary asteroid. The landing trajectory is designed by patching two trajectories of the external and internal CR3BP. More in detail, the landing phase is initiated when the spacecraft leaves the initial orbit exploiting its unstable manifolds, which drive the spacecraft towards the primary asteroid, up to the SOE. At the SOE, the transition from external to internal CR3BP occurs and a maneuver is performed to reach stable manifolds that drive the spacecraft towards the surface of the asteroid. A planar transfer case is compared to a full three-dimensional one.

Paragraphs 5.3.1 and 5.3.2 show trajectories computed respectively in the external and internal systems, while paragraph 5.3.3 presents the chosen landing solutions after patching external with internal trajectories.

5.3.1 Trajectories in the external CR3BP

It is assumed that initial orbits are imposed by mission requirements and constrained to keep the spacecraft permanently within the two asteroids, for observation purposes. For this reason, a lyapunov and a halo orbit about L1 are chosen as starting point for the planar and 3D landing solution (Figure 8).

To let the spacecraft reach the SOE from its initial orbit, unstable manifolds of both lyapunov and halo orbits are computed and propagated forward within their domain of validity (Figure 9). The unstable manifolds computed represent possible solutions for the first phase of the landing trajectory, from the initial orbit to the SOE.

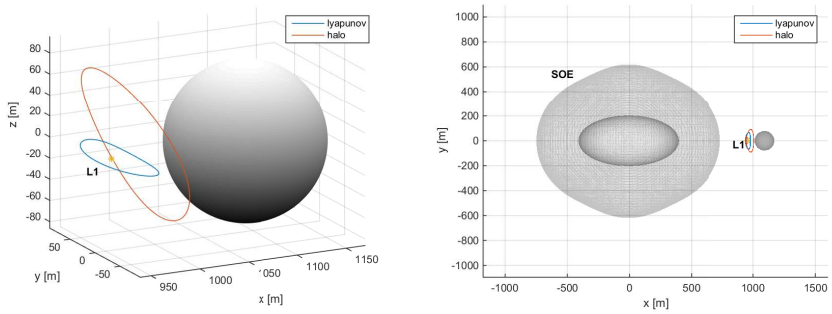

(a) (b)

Fig. 8 Initial orbits in the external CR3BP: lyapunov (planar case) and halo (3D case) orbits about the L1 point (a) close up view in the proximity of the smaller asteroid (b) x-y projection in the binary system

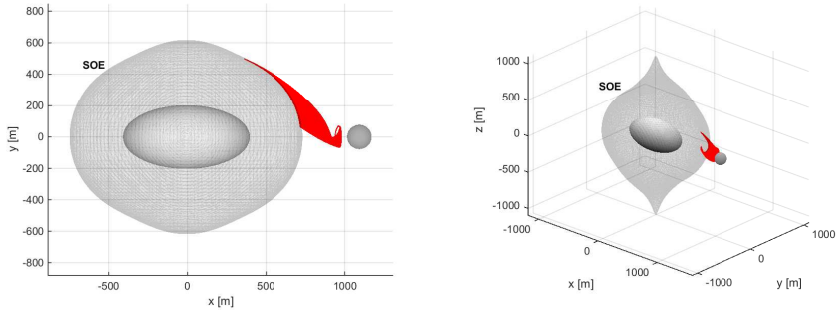

(a) (b)

Fig. 9 Unstable manifolds associated to (a) lyapunov and (b) halo orbits: forward propagation in the external CR3BP

5.3.2 Trajectories in the internal CR3BP

According to the patched three-body model in use, the dynamics of the spacecraft transition from external to internal CR3BP at the SOE. Trajectories in the internal CR3BP represent the last part of the landing trajectory, from the SOE to the surface of the primary asteroid. Landing points on the asteroid surface have been sought first, by computing periodic orbits in the internal CR3BP that intercept the surface of the primary. Figure 10 shows families of lyapunov and halo orbits about L2 in the internal CR3BP, which intersects the surface of the asteroids.

Suitable trajectories of the spacecraft from the SOE to the asteroid are found by computing stable manifolds associated to periodic orbits depicted in Figure 10. Manifolds are propagated backwards starting from identified landing points. Figure 11 shows computed stable manifold trajectories starting from suitable landing points, for both planar and three-dimensional cases.

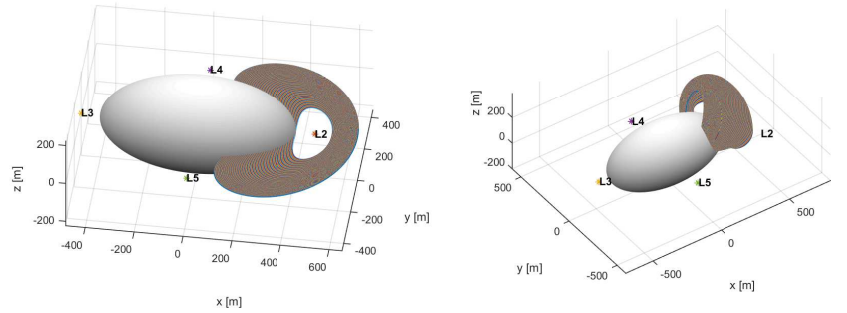

(a) (b)

Fig. 10 Families of (a) lyapunov and (b) halo orbits about L2 in the internal CR3BP: suitable landing points are identified by intersections with asteroid surface

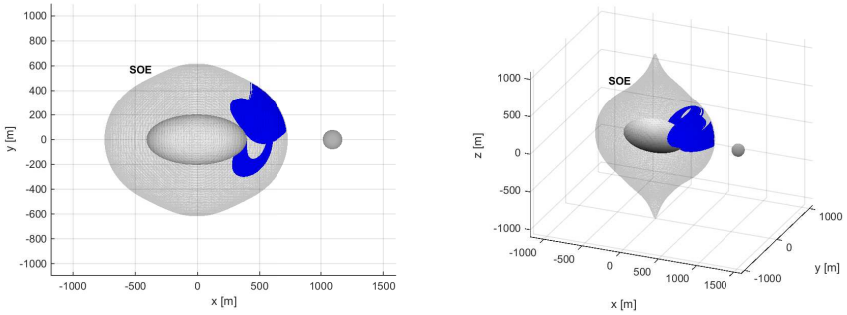

(a) (b)

Fig. 11 Stable manifolds associated to (a) lyapunov and (b) halo orbits: backward propagation from landing points in the internal CR3BP

5.3.3 Patched trajectories

Cost-effective landing solutions are investigated in this paragraph, after patching external with internal trajectories. A connection between unstable (external) and stable (internal) manifolds shall be found on the SOE. To this aim, Poicaré maps are used. Poincaré maps are widely used in dynamical system theory: examples of specific applications to astrodynamics problems can be found in Koon et al (2006). To patch internal and external trajectories, the SOE is taken as Poincaré section to compute the map.

The planar case is firstly discussed. Lyapunov orbits in internal and external CR3BP and their associated manifolds are considered here and shown in Figure 12(a).

Since all trajectories are planar, the full six-dimensional problem is reduced to four-dimensional. To find free connections between the stable and unstable manifolds, all four states x, $\dot{x}$, y, $\dot{y}$ of internal and external manifolds must match each other on the Poincaré section. However, the four states are not all independents as the location of the Poincaré section constrains one position state. Three states need to be matched at the SOE: one position state (x or y) and both velocity states ($\dot{x}$ and $\dot{y}$). To look at possible free transfers, two different Poincaré maps at the SOE have been built. Figure 13 shows the maps: red dots

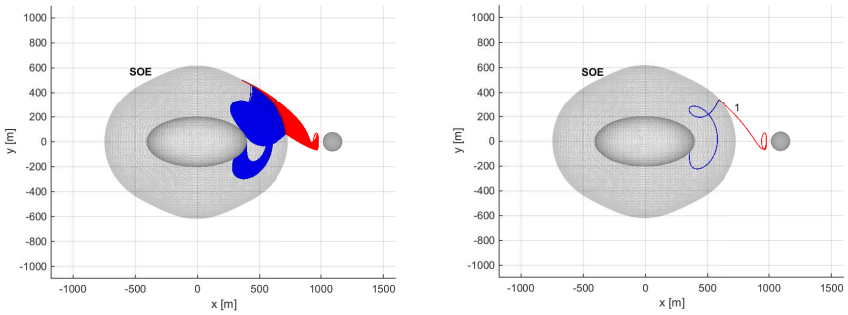

(a) (b)

Fig. 12 Unstable (red) and stable (blue) manifolds associated to external and internal CR3BP (planar case): (a) manifold families and (b) chosen solutions

represent unstable manifolds associated to the external CR3BP, while blue dots represent stable manifolds associated to the internal CR3BP.

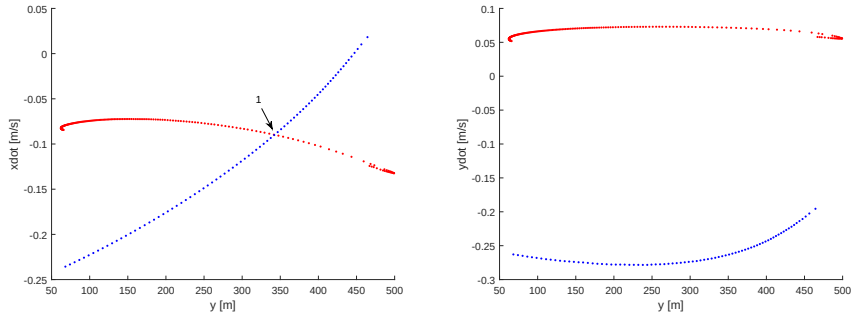

(a) (b)

Fig. 13 Poincaré maps associated to the planar landing case: (a) $y, \dot{x}$ and (b) $y, \dot{y}$. Red dots represent unstable (external) manifolds, blue dots represent stable (internal) manifolds

Figures 13(a) and 13(b) show the projection of manifolds on the SOE in the phase spaces $(y, \dot{x})$ and $(y, \dot{y})$. Stable and unstable manifolds have one intersection in the $(y, \dot{x})$ phase space, hence one point on the SOE exists where manifolds have the same position and the same $\dot{x}$. On the other hand, no intersections exist in the $(y, \dot{y})$ plane, and then, no points where the whole state of internal and external manifolds matches exist. Since no free transfer trajectories exist, a maneuver shall be performed on the SOE to match the $\dot{y}$ state. The intersection in Figure 13(a) is selected as possible landing solution and referred as solution 1 in the followings. Figure 12(b) shows the full trajectory associated to landing solution 1 in the x, y plane, as patched trajectory in external and internal systems. Table 2 reports the cost of the maneuver to be provided at the SOE, which in this case corresponds to a $\Delta\dot{y}$ maneuver.

The three-dimensional case is then discussed. Figure 14 shows computed manifolds associated to the three-dimensional case and their interaction on the SOE.

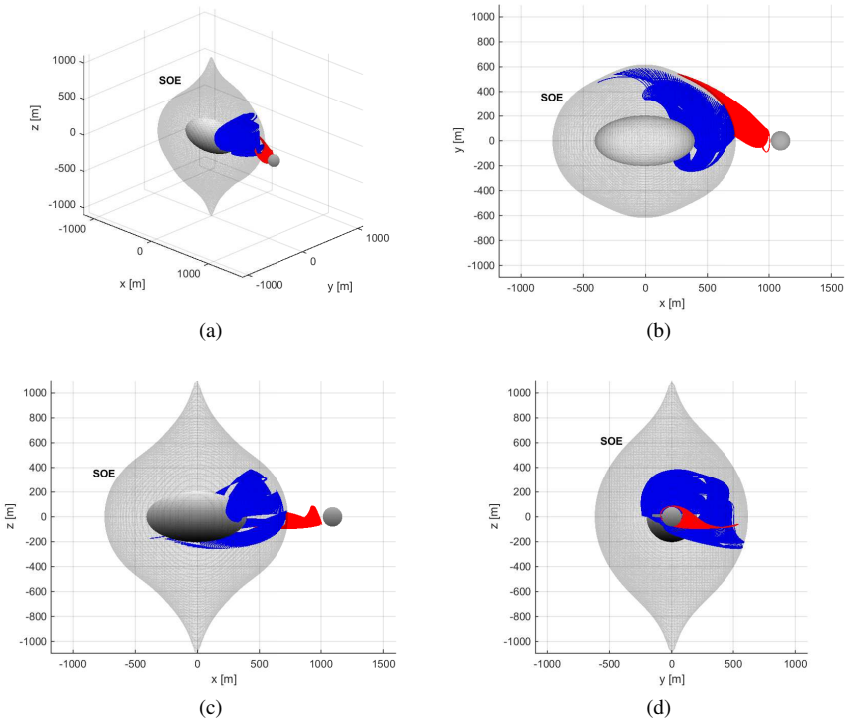

Fig. 14 Unstable (red) and stable (blue) manifolds associated to external and internal CR3BP (3D case): (a) three-dimensional view (b) x,y (c) x,z and (d) y,z projections

Table 2 Δv for selected landing solutions

ID landing solution	Δv [cm/s]
1 (2D)	33.7
2 (3D)	37.8
3 (3D)	39.4
4 (3D)	41.6

In this case, connection points are sought to guarantee continuity in position state between internal and external manifolds: three states are to be matched. The Poincaré section is again the SOE, which constraints one position state, and the map is built to represent x, y projection of manifolds on the SOE. Figure 15(a) shows the Poincaré map and the three intersections that exist between stable and unstable manifolds. These are referred as landing solutions 2, 3 and 4 in the followings. Blue dots in Figure 15(a) are shown to belong to four different curves, which correspond to four different kinds of families of stable manifolds associated to internal CR3BP solutions (Figure 11(b)).

The cost of the maneuver to be performed at the SOE is reported in Table 2 for all planar and three-dimensional selected solutions.

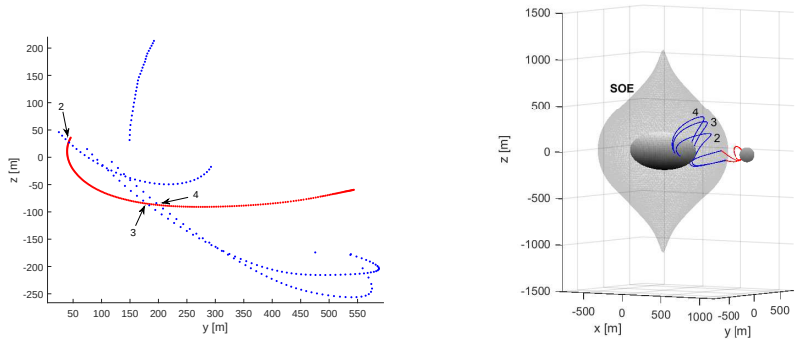

(a) (b)

Fig. 15 (a) Poincaré map associated to the 3D case: red dots represent unstable (external) manifolds, blue dots represent stable (internal) manifolds (projection in the x, y plane). (b) Selected landing solution for 3D case

5.4 Validity of the model and further refinement

The goal of the study is to demonstrate the effectiveness of the patched three-body approach presented here. For this reason, perturbing actions have not been included at this stage.

As a further step, disturbances such as Solar Radiation Pressure (SRP) and gravity of the Sun can be easily included, as well as more accurate models of the mass distribution of the asteroid (see section 1) to model to higher accuracy both the gravity field of the asteroid and the dynamics of the spacecraft.

Nevertheless, the model presented in this work, does effectively represent a binary NEA system under certain assumptions. Some of them are defined in section 3 such as mass distribution of the primary and relative kinematics of the system. Other assumption refer to the negligibility of perturbations. The most important source of orbital perturbation when flying a spacecraft about an asteroid is due to the presence of the Sun (SRP and gravity of the Sun). Concerning SRP, it is known that its effects become relevant when long-term missions are considered. In this work the dynamical model is used to compute short-time trajectories, hence the accuracy of the dynamics is not compromised by the absence of such an effect. Finally, the assumption of neglecting the gravity of the Sun is motivated by the fact that the mission analysis is confined within the Sphere Of Influence (SOI) of the binary system. The radius of the SOI is here computed according to its classical formulation (Roy 1988):

$$r_{\mathrm{SOI}} = r_{Sun}\left(\frac{m_A}{m_S}\right)^{\frac{2}{5}} = 8.61 \text{ km} \tag{22}$$

where m_A is the total mass of the binary system, m_S is the mass of the Sun and r_{Sun} is the distance of the binary from the Sun (data refer to Table 4 in appendix). As shown in Figure 7, the dynamical environment under study is confined well below the distance of 8.61 km from the barycenter of the binary system.

6 Conclusion

The dynamical model of a binary asteroid is built with a patched three-body approach. Relative kinematics between asteroids have been investigated for the case of binary systems and design parameters have been identified for the specific relative configuration under study. The dynamical model appears to be particularly suitable to model certain classes of bodies, which are very common among asteroid population, such as elongated and dog-bone shaped asteroids, as well as contact or close binaries. To confine regions of applicability of the patched three-body problems, the concept of SOE is introduced and defined. The dynamical model has been used to simulate possible mission scenarios aimed to the exploration of a NEA binary system. Cost-effective landing trajectories are identified by means of manifolds interaction between patched three-body problems, resolved through Poincaré analysis on the SOE.

The dynamical model defined in this work can serve as an easy and useful tool to identify trajectories in such complex dynamical scenarios. The patched three-body approach allows the exploitation of the peculiar dynamical properties of the CR3BP and cost-effective trajectories can be computed starting from periodic or quasi-periodic orbits and their invariant manifolds. The SOE, defined in this work, represents a tool to compare different vectorial fields: within the patched three-body approach, the SOE is exploited as a valuable alternative to the SOI, in case small and low-massive systems, such as asteroids, are considered as sources of gravity field.

When the assumptions on the distribution of mass in the binary system are valid, the physical system is well represented by the dual three-body model; hence it is possible to rely on its solution, avoiding the expensive computational effort required by higher fidelity models. The resulting trajectory can be used as a suitable first guess solution, to be differentially corrected towards higher fidelity model for further mission analysis refinements.

Appendix

Data in use throughout the paper are reported in here. A hypothetical target binary system has been selected among the wide binary NEA population (Johnston 2015): Table 3 reports the ranges of properties relevant for the case of study. Table 4 shows values in use in this study to model the target binary system and to assign the set of parameters $\boldsymbol{P}$.

Table 3 NEA binary population

	quantity	range of values
Asteroid couple	heliocentric semi-major axis	$[0.6-3]$ AU
	mass ratio	$[10^{-4}-10^{-1}]$
	distance between primaries	$[0.25-8]$ km
Primary asteroid	diameter	$[120-8200]$ m
Secondary asteroid	diameter	$[50-800]$ m

It is here remarked that in this work, the shape of the asteroids is important only for landing design: the sizes of primary and secondary asteroids refer to their representation as ellipsoid (or sphere), to approximate their surface for the design of the landing trajectory.

Table 4 Case of study

	quantity	symbol	Value
Asteroid couple	mass ratio	μ_{ext}	0.0065
	characteristic length	L^*_{ext}	1100 m
	relative orientation	θ_0	0°
	distance from the Sun	r_{Sun}	1.64 AU
	total mass	m_A	$4.59 \cdot 10^{11}$ kg
Primary asteroid	mass ratio	μ_{int}	0.5
	characteristic length	L^*_{int}	400 m
	size (ellipsoid semi-axis)	(a_x, a_y, a_z)	(400, 200, 200) m
Secondary asteroid	size (sphere radius)	R_2	75 m

References

Bate RR, Mueller DD, E WJ (1971) Fundamentals of Astrodynamics. Dover, New York

Bellerose J, Scheeres DJ (2008) General dynamics in the restricted full three body problem. Acta Astronautica 62:563–576

Belton MJS (1994) Galileo encouter with 951 gaspra: First pictures of an asteroid. Science 257:1647–1652

Belton MJS, Chapman CR, Veverka J, Klaasen KP, Harch A, Greeley R, Greenberg R, Head III JW, McEwen A, Morrison D, Thomas PC, Davies ME, Carr MH, Neukum G, Fanale FP, Davis DR, Anger C, Gierasch PJ, Ingersoll AP, Pilcher CB (1994) First images of asteroid 243 ida. Science 265:1543–1547

Benner LAM, Hudson RS, Ostro SJ, Rosema KD, Giorgini JD, Yeomans DK, Jurgens RF, Mitchell DL, Winkler R, Rose R, Slade MA, Thomas LM (1999) Radar observations of asteroid 2063 bacchus. Icarus 139:309–327

Cheng AF (2013) Aida: Test of asteroid deflection by spacecraft impact. In: Proceedings of the 44th Lunar and Planetary Science Conference, The Woodlands, TX, USA

Cheng AF, Michel P, Reed C, Galvez A, Carnelli I (2012) Dart: Double asteroid redirection test. In: Proceedings of the European Planetary Science Congress, Madrid, Spain

Cruikshank DP, Dalle Ore CM, Geballe TR, Rouch TL, Owen TC, Cash M, de Bergh C, K HW (2000) Trojan asteroid 624 hektor: Constraints on surface composition. Bull Am Astron Soc 32

Gabern F, Koon WS, Marsden JE (2006) Parking a spacecraft near an asteroid pair. Journal of Guidance, Control and Dynamics 29(3)

Gómez G, Koon WS, Lo MW, Marsden JE, Masdemont J, Ross SD (2004) Connecting orbits and invariant manifolds in the spatial restricted three-body problem. Nonlinearity 17:1571–1606

Gozdziewski K, Maciejewski AJ (1999) Unrestricted planar problem of a symmetric body and a point mass. triangular libration points and their stability. Celestial Mechanics and Dynamical Astronomy (75):251–285

Johnston R (2015) Johnston's archive. URL `http://johnstonsarchive.net/astro/asteroidmoons.html`

Koon WS, Lo MW, Marsden JE, Ross SD (2006) Dynamical Systems, the Three Body Problem and Space Mission Design. World Scientific

Margot JL, Nolan MC, Benner LAM, Ostro SJ, Jurgens RF, Giorgini JD, Slade MA, Campbell DB (2002) Binary asteroids in the near-earth object population. Science 296:1445–

1448
Merline WJ, Weidenschilling SJ, Durda DD, Margot JL, Pravec P, Storrs AD (2002) Asteroids do have satellites. Asteroids III, University of Arizona Press pp 289–312
Ostro SJ, Chandler JF, Hine AA, Rosema KD, Shapiro II, Yeomans DK (1990) Radar images of asteroid 1989 pb. Science 248:1523–1528
Ostro SJ, Rosema KD, Hudson RS, Jurgens RF, Giorgini JD, Winkler R, Yeomans DK, Choate D, Rose R, Slade MA, Howard SD, Mitchell DL (1995) Extreme elongation of asteroid 1620 geographos from radar images. Nature 375:474–477
Ostro SJ, Hudson RS, Rosema KD, Giorgini JD, Jurgens RF, Yeomans DK, Chodas PW, Winkler R, Rose R, Choate D, Cormier RA, Kelley D, Littlefair R, Benner LAM, Thomas LM, Slade MA (1999) Asteroid 4179 toutatis: 1996 radar observations. Icarus 137:122–139
Ostro SJ, Hudson RS, Nolan MC, Margot J, Scheeres DJ, Campbel DB, Magri C, Giorgini JD, Yeomans DK (2000) Radar observations of asteroid 216 kleopatra. Science 288:836–839
Richardson DC, Leinhardt ZM, Melosh HJ, Bottke Jr WF, Asphaug E (2002) Gravitational aggregates: Evidence and evolution. Asteroids III, University of Arizona Press pp 501–515
Roy AE (1988) Orbital Motion. Adam Hilger, Bristol
Schaub H, Junkins JL (2002) Analytical Mechanics of Aerospace Systems. American Institute Of Aeronautics & Astronautics
Scheeres DJ (1994) Dynamics about uniformly rotating triaxial ellipsoids: Applications to asteroids. Icarus 110:225–238
Scheeres DJ (2004) Stability of relative equilibria in the full two-body problem. Ann NY Acad Sci 1017:81–94
Scheeres DJ, Bellerose J (2005) The restricted hill full 4-body problem: Application to spacecraft motion about binary asteroids. Dynamical Systems: An International Journal 20(1):23–44
Scheeres DJ, Ostro SJ, Hudson RS, DeJong EM, Suzuki S (1998) Dynamics of orbits close to asteroid 4179 toutatis. Icarus 132:53–79
Szebehely V (1967) Theory of Orbits: The Restricted Problem of Three Bodies. Academic Press, New York and London
Werner RA, Scheeres DJ (1997) Exterior gravitation of a polyhedron derived and compared with harmonic and mascon gravitation representations of asteroid 4769 castalia. Celestial Mechanics and Dynamical Astronomy 65:313–344
Zuber MT, Smith DE, Cheng AF, Garvin JB, Aharonson O, Cole TD, Dunn PJ, Guo Y, Lemoine FG, Neumann GA, Rowlands DD, Torrence MH (2000) The shape of 433 eros from the near-shoemaker laser rangefinder. Science 289:2097–2101